Journal of Sound and Vibration 341 (2015) 1–15

Contents lists available at ScienceDirect

Journal of Sound and Vibration

journal homepage: www.elsevier.com/locate/jsvi

Experimental validation of virtual absorbed energy of piezoelectric patch actuators in decentralized velocity feedback control of a plate

Yicheng Yu, Hongling Sun*, Yin Cao, Fengyan An, Jun Yang

Key Laboratory of Noise and Vibration Research, Institute of Acoustics, Chinese Academy of Sciences, No. 21 North 4th Ring Road West, Beijing 100190, China

ARTICLE INFO

Article history:
Received 20 September 2014
Received in revised form
26 November 2014
Accepted 12 December 2014
Handling Editor: L.G. Tham
Available online 7 January 2015

ABSTRACT

Virtual absorbed energy of the piezoelectric patch actuator is a cost function for the optimal feedback gain which has been proved theoretically. Previously, simulations have shown that maximizing the virtual absorbed energy and minimizing the kinetic energy of the plate can obtain almost the same feedback gain. In this work, the performance of virtual absorbed energy is validated by experiments on the reduction of the vibration of a smart panel with decentralized control loops. Each control unit consists of a collocated piezoelectric patch actuator and accelerometer sensor with a single channel digital controller. The open loop sensor/actuator frequency response function with different physical parameters (such as dimensions of plate and actuator), has been analyzed numerically and experimentally, to enhance the stability of the control system. Since the system is not unconditionally stable, a digital phase lag compensator is designed to guarantee the stability for larger feedback gains. The stability of the multi-channel decentralized feedback control system has been assessed by the eigenvalue locus of the open loop transfer function matrix. The control effectiveness of the reduction of the panel kinetic energy has been assessed by error sensors.

1. Introduction

Decentralized velocity feedback control for a smart structure has been investigated by many authors [1–7]. Control gain is a key factor in decentralized velocity feedback control, which determines the performance and stability of the control system directly. There is an optimal feedback gain that can be obtained by minimizing the kinetic energy or the radiated sound energy of the flexible structures [1–3]. However, the physical information of the structure and its sound radiation generally cannot be acquired conveniently. Therefore, several researchers focused on this problem and proposed some other cost functions [4–7] to find the optimal feedback gain instead of minimizing the kinetic energy, such as maximizing the energy absorption of actuators [6,7].

For a force actuator, the energy absorption can be expressed as the product of the force of the actuator and its velocity at the mounting point, which can be measured directly when the actuator and sensor are collocated. Also references [8,9]

* Corresponding author.
E-mail address: hlsun@mail.ioa.ac.cn (H. Sun).

http://dx.doi.org/10.1016/j.jsv.2014.12.017
0022-460X/

investigated the relationship between the energy absorption of the voice-coil actuator and the kinetic energy of the plate, with decentralized feedback loops. It was proved numerically and experimentally that maximizing the energy absorption of the actuator has a similar feedback gain to minimizing the kinetic energy. Reference [10] further analyzed the energy absorption of force actuators both in frequency domain formulation and time domain formulation, to figure out the conditions under which the minimum of kinetic energy and the maximum of absorbed energy could match. Recently, reference [11] showed that the optimization of the natural frequencies of the inertial actuator, its mechanical damping and the feedback gain, that maximize the power absorbed by the controller or minimize the kinetic energy of the host structure, are equivalent. Hence, the energy absorption seems to be a very feasible cost function for decentralized feedback control. However, the mounting of inertial actuator generally requires relatively large mass to generate the needed force, which makes it not so convenient for controlling a thin plate, compared to the piezoelectric actuators. On the other hand, the energy absorption of the piezoelectric patch actuators, which is equal to the product of its moments and the corresponding angular velocity, usually cannot be measured directly.

Virtual absorbed energy of the piezoelectric patch actuator is a new cost function, proposed to obtain the optimal feedback gain which has been proved theoretically [12]. The virtual absorbed energy is derived from energy absorption by replacing the angular velocity with the velocity signal, and thus virtual absorbed energy can be expressed as the product of the amplitude of the line moment and the velocity signal from the velocity sensor which can be acquired by accelerometers. Compared to the kinetic energy or the sound radiation power, virtual absorbed energy is much easier to measure. Furthermore, simulations have shown that feedback gain minimizing the kinetic energy or maximizing the virtual energy absorption are nearly the same, when the disturbance is broadband white noise [12]. Also the effects of different excitation bandwidth are analyzed theoretically on the performances of kinetic energy and virtual energy absorption as cost functions.

In this work, the performance of virtual absorbed energy is validated by experiments on the reduction of the vibration of a smart panel with decentralized control loops. The experiments are based on a panel–cavity system, and the primary disturbance is broadband acoustical noise, as shown in Section 2. In Section 3, the virtual absorbed energy is investigated and compared to the kinetic energy for optimal gain by simulations and experiments with different bandwidth excitations.

After the optimal feedback gain is ascertained, the design of digital filter is discussed in Section 4. Since actuator–sensor pair cannot be completely collocated in practice, there is phase lag of the open loop frequency response function at higher frequencies, and hence the system is not unconditionally stable. Therefore, the open loop frequency response function is studied theoretically at the beginning of Section 4 and simulations and experimental results are presented. As analog phase lag compensator can enhance the stability of the control system but not well enough, thus a digital phase lag compensator is designed according to the open loop frequency response function so that larger feedback gains could be achieved. The stability of this system is assessed by the eigenvalues loci of the open loop transfer function matrix. Finally the multichannel decentralized feedback control with the virtual absorbed energy is implemented. Different conditions for feedback control are investigated in Section 5. The control results of the kinetic energy of the panel are presented in a frequency band of 1–1k Hz. The measurement of the control result has been carried out by error sensors mounted at the centers of the panel element.

2. Experimental system

In this work, decentralized velocity feedback control of a plate using piezoelectric patch actuator with virtual absorbed energy is investigated based on a panel–cavity system which is shown in Fig. 1. An aluminum panel is mounted on the rectangular cavity with rigid walls. The plate is clamped by a pair of rigid aluminum frames on the open side of the perspex

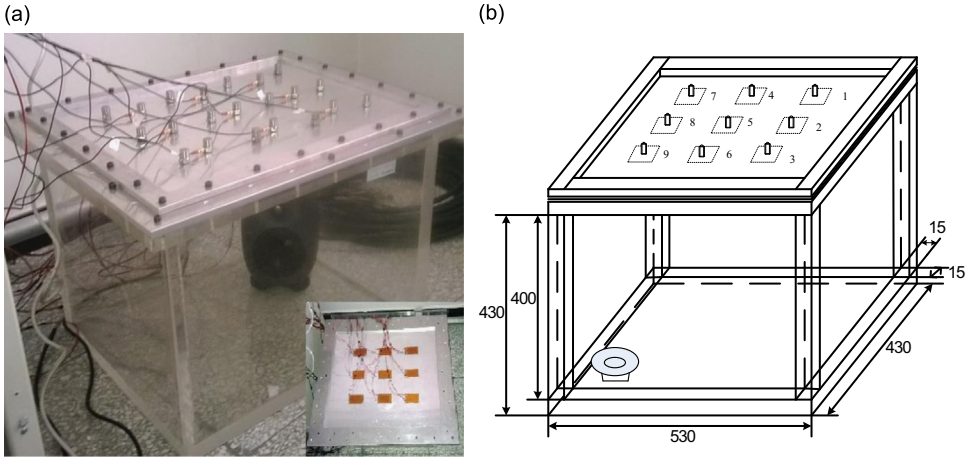

Fig. 1. The experimental facility of panel–cavity system: (a) aluminum panel with error sensors and 9 collocated sensor–actuator pairs and (b) simplified model.

box the boundary condition of which is between simply supported and clamped condition. At the corner of the box, there is a loudspeaker to generate the primary disturbance. A 3×3 array of piezoelectric actuators have been bonded on one side of the plate to generate bending moments. On the other side of the panel, a 3×3 array of accelerometer sensors numbered in Fig. 1(b) have been arranged corresponding to the centers of the piezoelectric actuators. The geometry and physical parameters of the plate, piezoelectric patches and transducers are presented in Tables 1–3.

As depicted in Fig. 1(a), the nine control accelerometers are placed on one side of the plate and the actuators on the other side. There are other 12 accelerometers used to measure the total kinetic energy of the plate. Each control unit consists of a collocated accelerometer (Lance, ULT2052) and piezoelectric patch actuator (Physik Instrumente, PI.P876), with a single channel digital controller. The digital system comprises an ADC (TI, ADS8422), a DAC (TI, DAC8820), and a FPGA (Alter, Cyclone III). The feedback control filter is accomplished in the FPGA, with the sample frequency of 1 MHz to produce less digital phase lag.

3. Experiments on virtual absorbed energy

Previously, the feasibility of virtual absorbed energy for optimal feedback gain in decentralized velocity control has been proved theoretically. In this work, experimental investigation on virtual absorbed energy is performed to confirm the theoretical research.

When the piezoelectric patch actuators are used as actuators, the energy they have absorbed is proportional to the moment induced by the piezoelectric patch actuators and the angular velocity of the plate. If replacing the angular velocity with the velocity signal, then there is a possibility for the quantity, which is the product of the amplitude of the line moment and the velocity signal from the velocity sensor, to be used to represent the energy absorption, and this quantity is termed the virtual energy absorption [12]. As the line moment of the actuator is nearly proportional to the output voltage of controller, therefore the total virtual absorbed energy of the piezoelectric patch actuators can be depicted as follows:

$$E_a = |\mathbf{u}_s^H \mathbf{v}_c| \tag{1}$$

where $\mathbf{u}_s$ is the output voltage vector of controllers; $\mathbf{v}_c$ is the velocity vector measured by the sensors; $(\cdot)^H$ denotes the Hermitian.

When the panel is disturbed by any broadband white noise from the speaker in the cavity, the velocity at the element centers and control points can be derived as

$$\mathbf{v}_e(\omega) = \mathbf{d}_e(\omega) + \mathbf{H}_{es}(\omega)\mathbf{u}_s(\omega) \tag{2}$$

$$\mathbf{v}_c(\omega) = \mathbf{d}_c(\omega) + \mathbf{H}_{cs}(\omega)\mathbf{u}_s(\omega) \tag{3}$$

where $\mathbf{v}_e(\omega)$ and $\mathbf{v}_c(\omega)$ are the velocity vectors at the element centers and control points, respectively. Likewise, $\mathbf{d}_e(\omega)$ and $\mathbf{d}_c(\omega)$ are the initial velocity vectors at the element centers and control points respectively, when there is only the acoustic disturbance without control. $\mathbf{H}_{es}(\omega)$ and $\mathbf{H}_{cs}(\omega)$ are the frequency response functions from the piezoelectric amplifier input to the output of accelerometer sensors at the element centers and control points respectively.

Table 1
Geometry and physical constants of the panel.

Parameters	Value
Dimensions	$l_x \times l_y = 500 \times 400\ \text{mm}^2$
Thickness	$h_s = 1.8\ \text{mm}$
Density	$\rho_s = 2700\ \text{kg/m}^3$
Young's modulus	$E_s = 7 \times 10^{10}\ \text{N/m}^2$
Poisson ratio	$\nu_s = 0.33$
Loss factor	$\eta_s = 0.05$
Smeared mass density	$\bar{\rho}_s = 2900\ kg/m^3$
Smeared Young's modulus	$\bar{E}_s = 7.4 \times 10^{10}\ N/m^2$

Table 2
Geometry and physical constants of the piezoelectric patches.

Parameters	Value
Dimensions	$a_x \times a_y = 61 \times 35\ \text{mm}^2$
Thickness	$h_p = 0.4\ \text{mm}$
Mass	$m_p = 2.1\ \text{g}$
Young's modulus	$E_p = 1.64 \times 10^{10}\ \text{N/m}^2$
Poisson ratio	$\nu_p = 0.35$
Strain constant	$d_{31} = 1.66 \times 10^{-10}\ \text{m/V}$

Table 3
Geometry and physical constants of the accelerometers.

Parameters	Value
Mass of the accelerometer case	$m_{ac}=0.2\times10^{-3}$ kg
Inertia mass of the accelerometer	$m_{ac}=0.2\times10^{-3}$ kg
Internal stiffness of the accelerometer	$k_a=1.1\times10^{7}$ N/m
Damping coefficient of the accelerometer	$c_a=2.5$ N/ms

When the control loop is implemented, the output voltage of controllers can be expressed as

$$\mathbf{u}_s = -\mathbf{H}(\omega)\mathbf{v}_c(\omega) \tag{4}$$

Here $\mathbf{H}(\omega)$ denotes the controller, which includes the designed feedback control filter, the analog filter of the digital system, and the delay of digital sampling. It should be noted that $\mathbf{H}(\omega)$ is a diagonal matrix for the decentralized control method.

Hence, the velocity at the element centers can be derived as

$$\mathbf{v}_e(\omega) = \mathbf{d}_e(\omega) - \mathbf{H}_{es}(\omega)\mathbf{H}(\omega)[\mathbf{I}+\mathbf{H}_{cs}(\omega)\mathbf{H}(\omega)]^{-1}\mathbf{d}_c(\omega) \tag{5}$$

The kinetic energy of the plate is given by

$$E_k(\omega) = \frac{m}{2N}\mathbf{v}_e^H(\omega)\mathbf{v}_e(\omega) \tag{6}$$

Here m is the mass of the plate and N is the number of the element.

The virtual absorbed energy is given by

$$E_a(\omega) = \mathrm{diag}(\mathbf{H}(\omega)\cdot[\mathbf{I}+\mathbf{H}_{cs}(\omega)\mathbf{H}(\omega)]^{-1}\mathbf{d}_c(\omega))^H\cdot[\mathbf{I}+\mathbf{H}_{cs}(\omega)\mathbf{H}(\omega)]^{-1}\mathbf{d}_c(\omega) \tag{7}$$

According to Eqs. (5)–(7), the kinetic energy and the virtual absorbed energy can be obtained by the measured plant frequency response functions and the plate original disturbance.

Previous simulations have shown that the virtual absorbed energy can be used to predict the optimal feedback gain in the case of broadband white noise excitation. In addition, when the bandwidth is reduced and does not include any resonance peaks, the virtual absorbed energy and kinetic energy do not have any direct relationship for optimal feedback gain [12]. Here the numerical and experimental comparison results of the virtual absorbed energy and the kinetic energy against different bandwidth excitation are presented.

3.1. Broadband excitation

In this experiment, the excitation is broadband white noise (bandwidth is 1–1k Hz). Numerical results of the kinetic energy and the virtual absorbed energy by control unit 6 and 8 as functions of the two feedback gains are given in Fig. 2. It shows that the optimal feedback gains maximizing the virtual absorbed energy and minimizing the kinetic energy are nearly the same in two channels feedback control. It can be noted that the optimal feedback gains of channel 6 and channel 8 are about 7 dB and 8 dB, respectively (which are calculated by 20 $\log_{10}$(Gain)). And it can be noticed that the optimal gain of a certain control unit does not change with the other channels' feedback gains, which have been proved previously in simulations [12]. Thus the optimal feedback gain of each control unit can be found with their own virtual energy absorption. Fig. 3 depicts the variation of the kinetic energy and the virtual energy absorption against the variation of each feedback gain, under the condition of the other eight feedback units working with almost the optimal feedback gain. Unit 5 is located at the center of the panel and unit 7 is located at the corner of the panel. And the other seven control units share the same conclusion. Therefore, in the case of nine control feedback units working simultaneously, minimizing the virtual absorbed energy and maximizing the kinetic energy can get almost the same feedback gain. The optimal feedback gain of each control unit can be seen in Fig. 3. The virtual absorbed energy in Figs. 2 and 3 are normalized by dividing its maximum between the feedback gain band width of -20 dB $\sim$20 dB. The same process also takes place for the kinetic energy. It should be noted that the virtual absorbed energy and the kinetic energy are obtained by measuring the practical transfer functions and primary disturbance, and then calculating with Eqs. (5)–(7), while reference [12] gave the results with theoretical transfer functions. In this experiment, when the feedback gain is too large, the control system will get unstable at higher frequencies, and the virtual absorbed energy and the kinetic energy cannot be measured directly.

3.2. Different bandwidth excitation

Reference [12] found that, when the excitation bandwidth is reduced to not include any vibration resonance peaks, the virtual absorbed energy of the actuator is not suitable to be the cost function. In this work, the corresponding experimental results with different number of control loops are carried out. Experimental results for nine channel feedback control are given in Fig. 4. Fig. 4(a) depicts the difference of feedback gain of channel 7 against excitation bandwidth variation between

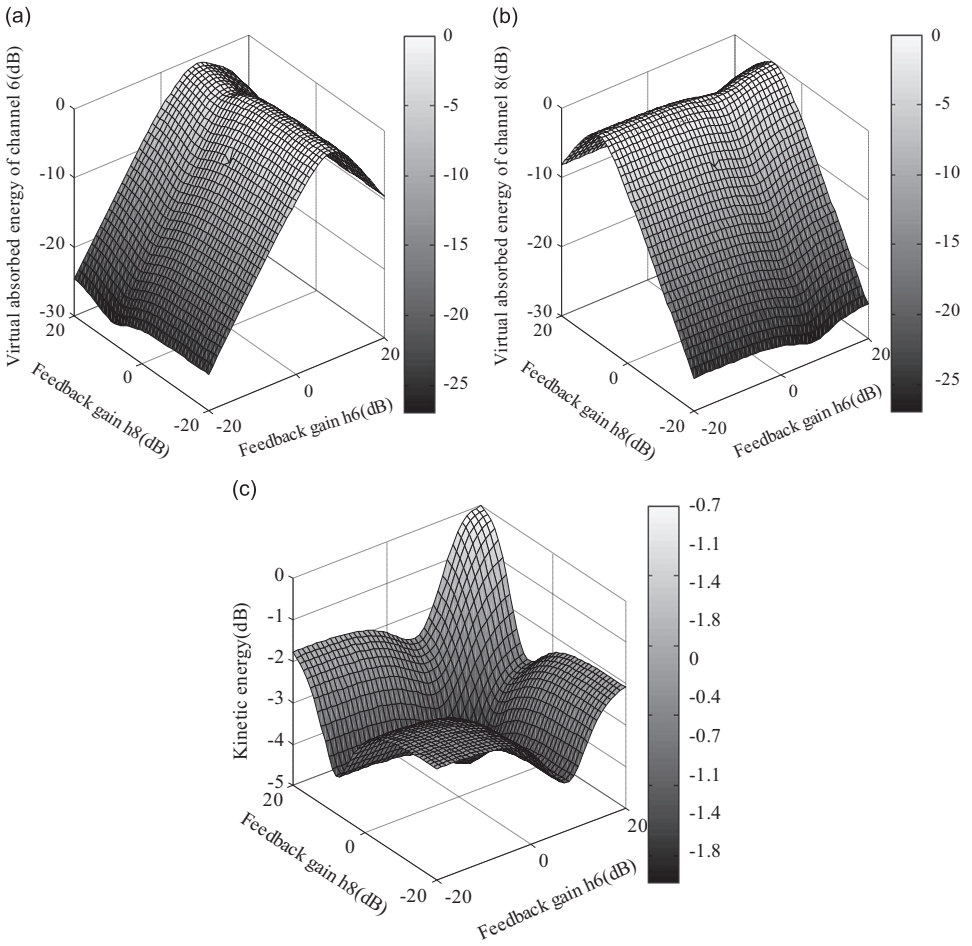

Fig. 2. Numerical results of the kinetic energy and the virtual absorbed energy by control unit 6 and 8 as functions of the two feedback gains: (a) the variation of the virtual absorbed energy of unit 6 towards the variation of the two feedback gains; (b) the variation of the virtual absorbed energy of unit 8 towards the variation of the two feedback gains; (c) the variation of the kinetic energy towards the variation of the two feedback gains.

minimizing the kinetic energy and maximizing the virtual absorbed energy when nine control units working. Fig. 4(b) shows the difference of the kinetic energy of the panel between these two situations. The excitation bandwidth changes from 1 Hz to 1k Hz, and the start frequency is 1 Hz.

It can be noticed from Fig. 4 that when the frequency bandwidth is smaller than 73 Hz, the difference of feedback gain between the two situations is large, so is the kinetic energy; however, when the frequency bandwidth exceeds 73 Hz, the difference of feedback gain or the kinetic energy is small, which have been studied theoretically previously [12]. A detailed analysis of the response of the plate shows that 73 Hz is the new first peak of the panel when the control unit with large feedback gains is added to the system. This could be imagined that at low frequencies, large feedback gain is needed so that the control loop will pin the panel at the control position [2,5], and thus minimizing the kinetic energy of the panel, like a single dof system. On the other hand, when the feedback gain is too high, the response of the panel at the control point is close to zero, and hence the virtual absorbed energy is also close to zero. Therefore, maximizing the virtual absorbed energy does not work [12].

4. Digital feedback controller design and implementation

The multichannel decentralized velocity feedback control system can be depicted in Fig. 5. The matrix $\mathbf{G}(j\omega)$ denotes the open loop frequency response function, which is the transfer function between the actuator amplifier input and the accelerometer sensor output of this system. $\mathbf{H}(j\omega)$ is the feedback filter which contains the feedback gain and the phase lag compensator. Before the multichannel feedback control is implemented, the stability of the system has to be ensured. In order to guarantee the stability of the control system for larger feedback gains, the collocation of the sensor–actuator pair ought to be improved, such as changing the parameters of the experimental system and also the control performance could be enhanced by shaping the control function with compensator. The open loop sensor/actuator transfer function is analyzed

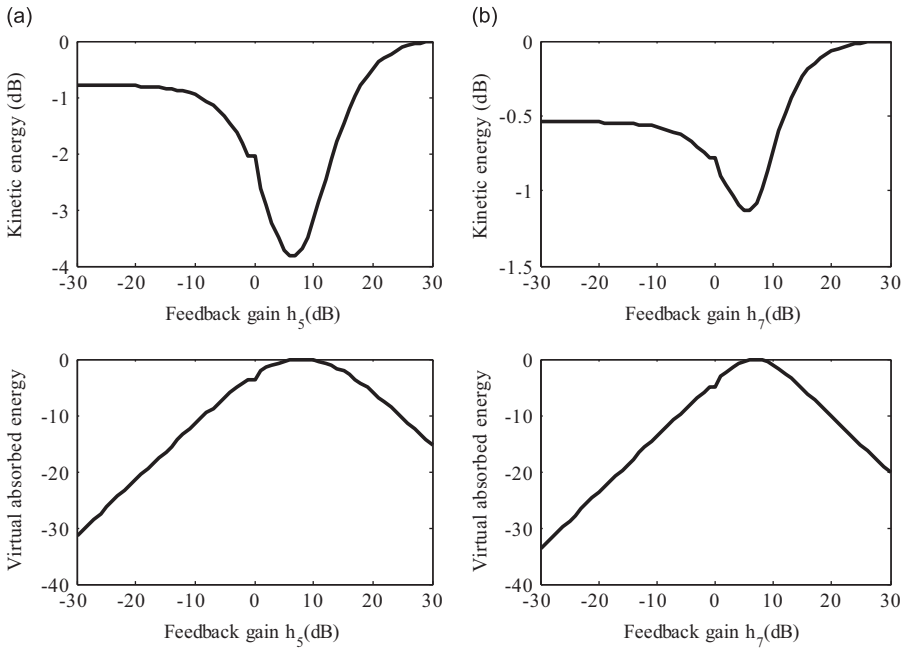

Fig. 3. The variation of the kinetic energy and the virtual energy absorption against the variation of the feedback gain of control unit $5h_5$ and unit $7h_7$. (a) Unit 5 and (b) unit 7.

in experiments and simulations, and the compensator is designed according to the open loop frequency response function, which will be introduced later in this section.

4.1. Mathematical model of open loop frequency response function

When the actuator and sensor are collocated, the open loop frequency response function has some particular properties. At low frequency band, the phase of the frequency response function is between 0° and 180° (because the accelerometer sensor has a phase lead of 90° compared with the velocity sensor), which can be used to guarantee the stability of the direct feedback control system. However, at higher frequencies, the open loop frequency response function is not strictly positive real, which will reduce the performance capability of the system. The collocation of the sensor–actuator pair is studied numerically and experimentally in the following section.

The open loop frequency response function is influenced by the dynamic parameters of the accelerometer transducers and piezoelectric patch actuators, the coupled effect of the cavity, and the plate vibration response. The equations are given by Gardonio and Bianchi [13], where the mass effect of the piezoelectric patches has been smeared over the plate, thus the Young's modulus and density parameters of the plate are modified.

$$\mathbf{v}_c(\omega) = \mathbf{T}_{cs}(\omega)\mathbf{f}_s(\omega) \tag{8}$$

where $\mathbf{v}_c(\omega)$ and $\mathbf{f}_s(\omega)$ denotes the phasors of the transverse velocities and moments acting on the control unit. $\mathbf{T}_{cs}(\omega)$ is given by

$$\mathbf{T}_{cs} = (\mathbf{I}+\mathbf{Y}_{cc}\mathbf{Z}_{aa}-\mathbf{Y}_{ce}\mathbf{Z}_{bb}(\mathbf{I}+\mathbf{Y}_{ee}\mathbf{Z}_{bb})^{-1}\mathbf{Y}_{ec}\mathbf{Z}_{aa})^{-1}(\mathbf{Y}_{cs}-\mathbf{Y}_{ce}\mathbf{Z}_{bb}(\mathbf{I}+\mathbf{Y}_{ee}\mathbf{Z}_{bb})^{-1}\mathbf{Y}_{es}) \tag{9}$$

where the components of the velocity/force mobility matrices, $\mathbf{Y}_{cc}$, $\mathbf{Y}_{ce}$, $\mathbf{Y}_{ee}$, $\mathbf{Y}_{ec}$, between the velocities at position (x_i, y_i) and forces at (x_k, y_k), are given by

$$Y^{i,k}(\omega) = \frac{v_i(\omega)}{f_k(\omega)} = j\omega \sum_{m=1}^{M}\sum_{n=1}^{N} \frac{\phi_{mn}(x_i,y_i)\phi_{mn}(x_k,y_k)}{\Lambda_{mn}[\omega_{mn}^2(1+j\eta_s)-\omega^2]} \tag{10}$$

and the components of velocity/moment matrices, $\mathbf{Y}_{cs}$ and $\mathbf{Y}_{es}$, between the velocities at position (x_i, y_i) and bending moments per unit width of the actuator at $(x_{k1}, y_{k1}; x_{k2}, y_{k2})$, are given by [14]

$$Y_s{}^{i,k}(\omega) = \frac{v_i(\omega)}{m_k(\omega)}$$

$$= j\omega \sum_{m=1}^{M}\sum_{n=1}^{N} \frac{4(k_m^2+k_n^2)(\cos\ k_m x_{k2} - \cos\ k_m x_{k1})(\cos\ k_n y_{k2} - \cos\ k_n y_{k1})}{\rho_s h_s l_x l_y k_m k_n[\omega_{mn}^2(1+j\eta_s)-\omega^2]} \sin(k_m x_i)\sin(k_n y_i) \tag{11}$$

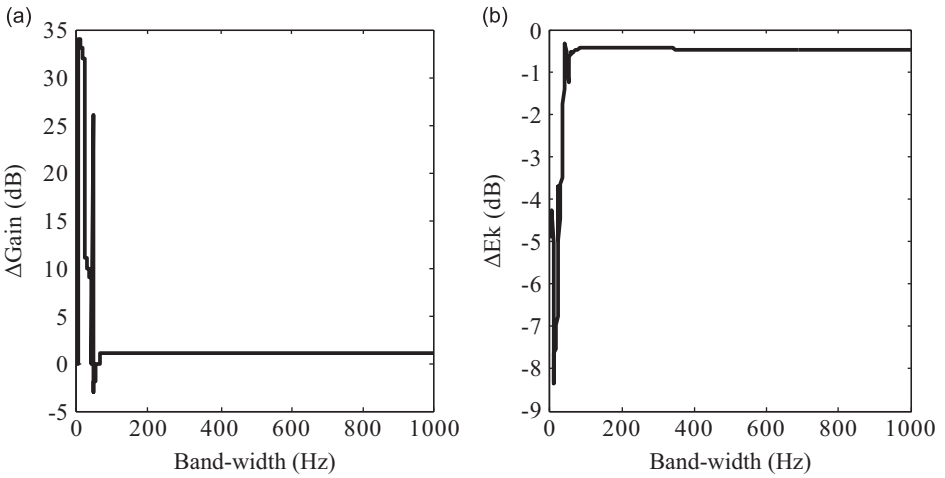

Fig. 4. Nine channels feedback control. (a) The difference of the feedback gains of channel 7 against bandwidth between minimizing the kinetic energy and maximizing the virtual absorbed energy with the other feedback loop working. (b) The difference of the kinetic energy against bandwidth in the same two situations as (a).

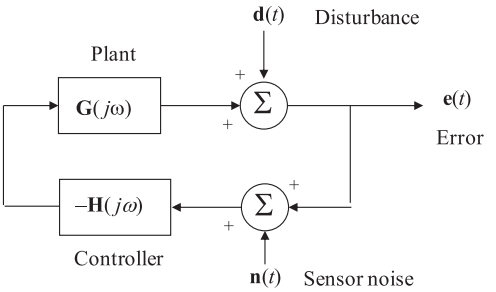

Fig. 5. The block diagram of the multichannel decentralized velocity feedback control system.

where m and n are the modal indices, ω_{mn} the natural frequency of the (m, n)th mode, $\phi_{mn}(x,y)$ the (m, n)th panel mode shape (for simply supported plate $= \sin(mx/l_x)\sin(ny/l_y)$), Λ_{mn} the modal mass of the (m, n)th mode $(=\rho_s h_s l_x l_y/4)$, ρ_s the density of the plate, h_s the thickness of the plate, η_s the hysteresis loss factor, a_x, a_y the dimensions of the piezoelectric patch, x_{k1}, x_{k2} the x-position of the two a_y edges of the kth piezoelectric patch, and y_{k1}, y_{k2} the y-position of the two a_x edges of the kth piezoelectric patch.

And the component of the force/velocity impedance matrices $\mathbf{Z}_{bb}$, between the transverse forces at the centers of the elements on the top side of the cavity at position (x_i, y_i, l_{zb}), and the velocities at position (x_k, y_k, l_{zb}), are given by

$$Z_{bb}^{i,k}(\omega) = \sum_{r=1}^{R}\sum_{s=1}^{S}\sum_{t=1}^{T} \frac{\omega\rho_0 c_0^2 \Delta S^2 \chi_{rst}(x_i, y_i, l_z)\chi_{rst}(x_k, y_k, l_z)}{\Lambda_{rst}[2\zeta_{rst}\omega_{rst}\omega + j(\omega^2 - \omega_{rst}^2)]} \tag{12}$$

where r, s, and t are the modal indices, ω_{rst} the natural frequency of the (r, s, t)th mode, $\chi_{rst}(x,y,z)$ the (r, s, t)th cavity mode shape, Λ_{rst} the modal normalization parameter $(=l_x l_y l_z)$, ρ_0 the density of air, c_0 the speed of sound in air, ς_{rst} the damping ratio of the (r, s, t)th mode, and ΔS is the area of the elements.

The force/velocity impedance matrix $\mathbf{Z}_{aa}$ is diagonal:

$$\mathbf{Z}_{aa} = \begin{bmatrix} Z_{eq1} & & & & \\ & Z_{eq2} & & & \\ & & Z_{eq3} & & \\ & & & \cdots & \\ & & & & Z_{eq9} \end{bmatrix} \tag{13}$$

where Z_{eqj} is given by

$$Z_{eqj} = f_{aj}/v_{aj} = \frac{1 - T(\omega)}{Y_1(\omega)} \tag{14}$$

and

$$T(\omega) = -Y_1(\omega)Z_{m11}(\omega) + \frac{Y_1(\omega)Z_{m12}(\omega)Y_2(\omega)Z_{m21}(\omega)}{1+Y_2(\omega)Z_{m22}(\omega)} \tag{15}$$

$$Y_2(\omega) = \frac{1}{j\omega m_a} \tag{16a}$$

$$Y_1(\omega) = \frac{1}{j\omega m_{ac}} \tag{16b}$$

$$Z_{m11}(\omega) = \left(c_a + \frac{k_a}{j\omega}\right) \tag{17a}$$

$$Z_{m12}(\omega) = -\left(c_a + \frac{k_a}{j\omega}\right) \tag{17b}$$

$$Z_{m21}(\omega) = -\left(c_a + \frac{k_a}{j\omega}\right) \tag{17c}$$

$$Z_{m22}(\omega) = \left(c_a + \frac{k_a}{j\omega}\right) \tag{17d}$$

The geometry and physical constants of the plate, piezoelectric patch and the accelerometer transducer are presented in Tables 1–3.

The output voltage of the accelerometer a_{mea} is different from the velocity at the mounting point of the plate v_c, and the relation between them is given by [15]

$$a_{mea}(\omega) = M(\omega)v_c(\omega) \tag{18}$$

where

$$M(\omega) = j\omega\frac{sm_a}{k_a - m_a\omega^2 + jc_a\omega} \tag{19}$$

and s is the sensitivity of the accelerometer.

Also, if the piezoelectric patch actuator is large enough compared to its thickness, the bending moments induced by the actuator can be regarded as four line moments at its edges [16]. The bending moments in the plate per unit length is proportional to the input voltage of the amplifier of the piezoelectric patch V, and is given by [17] (for the case of zero glue layer thickness)

$$M_x = M_y = C_0\frac{d_{31}V}{h_p} \tag{20}$$

where C_0 is a constant associated with the characteristics of the piezoelectric patch actuator and the plate:

$$C_0 = \frac{\rho_a(2+\rho_a)}{4(1+\beta\rho_a(3+\rho_a^2+3\rho_a))}h_p^2\gamma \tag{21}$$

and

$$\rho_a = 2h_p/h_s \tag{22a}$$

$$\beta = \frac{(1-\nu_s)E_p}{(1-\nu_p)E_s} \tag{22b}$$

$$\gamma = \frac{E_p}{1-\nu_p} \tag{22c}$$

Hence, the expression of the moments can be obtained by

$$\mathbf{f}_s = A(\omega)\frac{C_0 d_{31}}{h_p}\mathbf{u}_s \tag{23}$$

where $A(\omega)$ is the transfer function of the amplitude of the piezoelectric patch actuator and $\mathbf{u}_s$ is the input voltage of the amplitudes.

The expression of the open loop frequency response function $\boldsymbol{G}(\omega)$ can be obtained by equation expressions (8), (18) and (23) to give

$$\mathbf{a}_{mea} = M(\omega)A(\omega)\frac{C_0 d_{31}}{h_p}\mathbf{T}_{cs}(\omega)\mathbf{u}_s = \mathbf{G}(\omega)\mathbf{u}_s \tag{24}$$

4.2. Experiments and Simulations on open loop frequency response function

In this section, the open loop frequency response function has been analyzed in simulations and experiments, to figure out the main factors which determine its phase lag at higher frequencies. The effects of physical parameters of the plate, actuator and transducer are investigated.

First of all, the simulation of the open loop frequency response function has been compared with the experimental one at the frequency band of 1–10k Hz, as shown in Fig. 6. The dotted line, which represents the simulated transfer function as depicted in Eq. (24), overlaps with the measured one for the first several resonances. Moreover the phase lags of the simulated and measured frequency response functions have the same tendency. The difference between them may be induced by the deviation of some dynamic approximation. Hence, the simulation can be applied to predict the open loop frequency response function. It should be noted that the resonance peaks of the simulated open loop transfer function are more conspicuous than the measured ones, which may be caused by some error of the simulated parameters, such as the loss factor.

The effect of the factors on open loop frequency response function phase lag has been studied as follows.

4.2.1. Dimensions of piezoelectric patch actuator

As the piezoelectric patch actuator generates four line moments at its edges, and the accelerometer is mounted at the center of the actuator, the actuator–sensor pair is not strictly collocated [18-21], which will give rise to the phase lag of the frequency response function at higher frequencies. Hence, Gardonio [13] has used smaller actuator to enhance the collocation of the actuator–sensor pair.

Actually the thickness of the piezoelectric patch can also influence the phase lag of the transfer function. With the increasing thickness of the actuator, the mass of the actuator will generally increase, contributing to the raising smeared mass density and smeared Young's modulus of the panel, which will change the phase lag of the transfer function. Also, for constant applied electric field strength, there exists an optimal actuator thickness for active control [16], and this can be calculated using Eq. (20). The optimal actuator thickness is about a quarter of the aluminum panel thickness. In this experiment, the comparison of different thickness actuators have been investigated, and the results of the open loop frequency response functions are shown in Fig. 7. The piezoelectric patch is made by Physik Instrumente (PI), and the two different actuators are P-876-A11 (0.4 mm) and P-876-A15 (0.8 mm) respectively. Fig. 7 shows that the amplitude–frequency responses of the two transfer functions are almost the same, because the thicker actuator (A15) has higher Young's modulus ($E_p = 34.7 \times 10^{10}\ N/m^2$), thus it can generate almost the same bending moment as the standard one (A11), namely the constant C_0/h_p in Eq. (20) is almost the same. Although the increasing smeared Young's modulus and density of the plate is

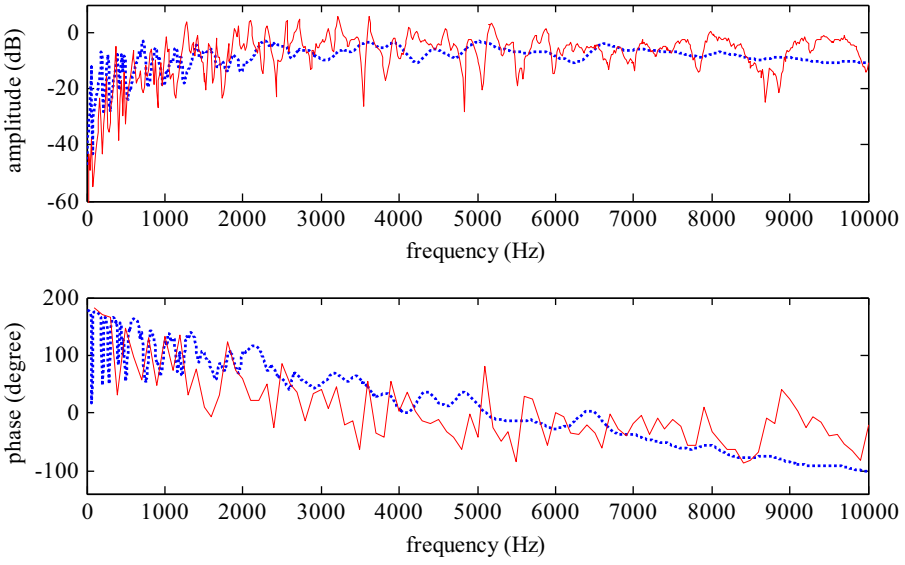

Fig. 6. Open loop frequency response function of a sensor/actuator pair (1–10k Hz). Simulated FRF (dashed line) and measured FRF (solid line).

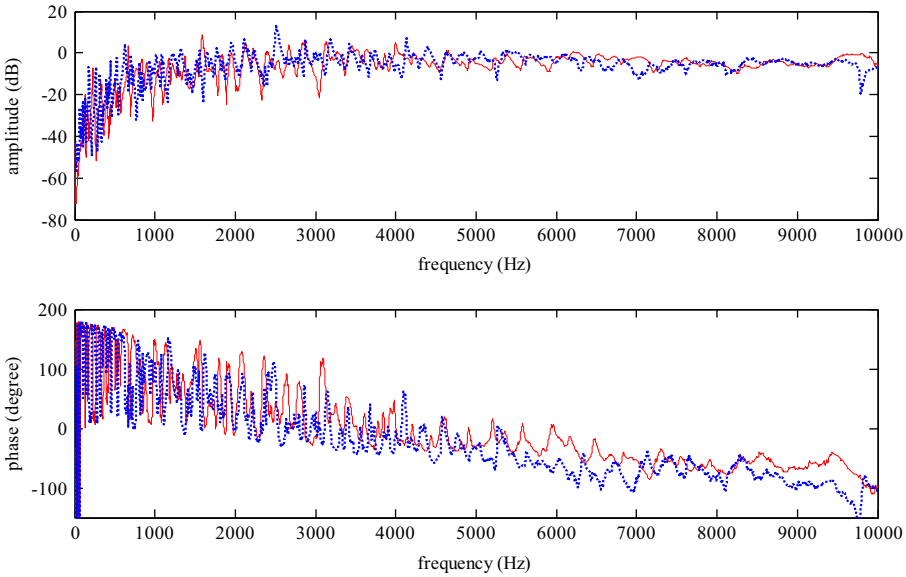

Fig. 7. Experimental open loop frequency response function of a sensor/actuator pair (1–10k Hz). Thicker actuator with higher Young's modulus and density (dashed line), standard actuator (solid line).

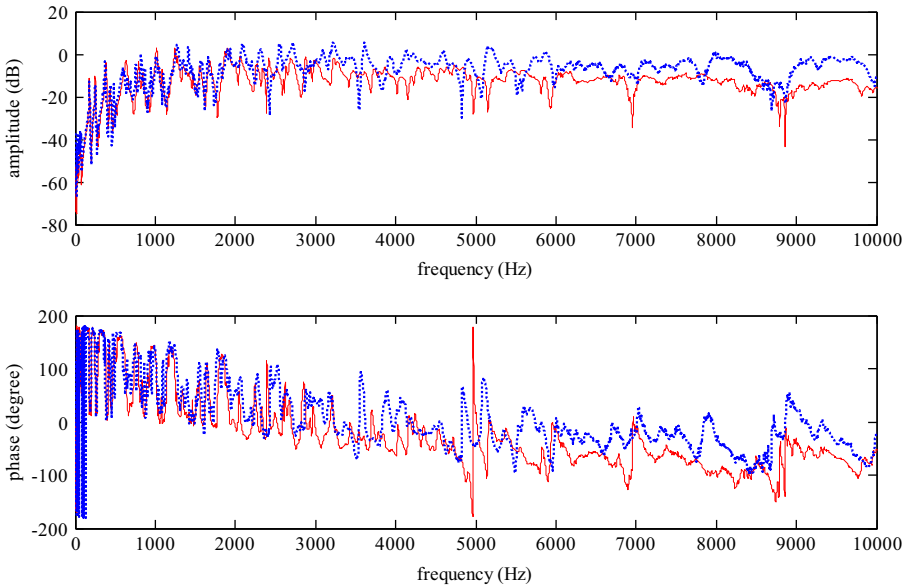

Fig. 8. Experimental open loop frequency response function of a sensor/actuator pair (1–10k Hz). Standard transducer (dashed line) and bigger transducer (solid line).

relatively small, it can still produce an extra phase shift, which is shown in Fig. 7. Moreover the corresponding simulations have also been carried out and have the same tendency which are not given here for brevity. The probable reason for the extra phase shift is that the increasing mass of the actuator raises the reactance of the system especially at higher frequencies. This phenomenon becomes more conspicuous when the mass of the transducer increases.

4.2.2. The mass of the accelerometer transducer

The mass of the transducer acts as a low-pass filter for the open loop frequency response function. It can be imagined if we simplify the panel–transducer system as a single dof system. At lower frequencies, the mechanical compliance is the main impedance of the system. Hence, the increasing mass of the transducer does not have any impact on the transfer function. However, at higher frequencies, the increasing mass will produce conspicuous increasing impedance of the system, and suppress the vibration response of the panel, so as to reduce the amplitude of the transfer function and increase the

phase shift. The experimental results are presented in Fig. 8. The standard transducer is made by PCB Piezotronics (model 352C67), and the bigger transducer is made by Lance (ULT2052). There is a singular point in the frequency–phase response plot at about 5000 Hz, which is probably because the transfer function at this point is not correctly measured, or the signal-to-noise-ratio is not high enough.

Although using smaller transducer can efficiently reduce phase lag of the open loop frequency response function, the amplitude of the transfer function also increases meanwhile, which is almost equivalent to increasing the gain of the feedback loop, and requires the feedback filter increasing the reduction of its amplitude at higher frequencies. Thus a compromise should be found between the reduction of the phase lag and the increasing of the amplitude of the open loop frequency response function. Similarly the simulations of the open loop frequency response function of different transducers have the same tendency as the experimental one.

4.2.3. Dimensions of the plate

It can be imagined that when the thickness of a thin panel increases, the natural frequencies of the panel and its modal mass will also increase, which will reduce the phase lag of the transfer function Y_{cs} (Eq. (11)). On the other hand, with reducing the thickness of the panel, the coupling of the cavity and the panel will generally be stronger, therefore the transverse force from the coupling cavity acting at the panel will get more considerable. Thus the actuation and the sensing are "more non-collocated", and this can probably produce a phase shift of the open loop frequency response function. The experimental results are shown in Fig. 9. The phase response shown in Fig. 9 has many singular points at some higher frequencies. This is probably because the experimental panel is not flat enough, and the signal-to-noise ratio is a little bit low. However, the tendency of the experimental or simulated phase frequency response shows the thicker panel produces less phase lag, if the plate satisfies the thin-plate assumption.

4.3. Filter design

Because the open loop frequency response function is not strictly positive real at higher frequencies, and additionally, the digital system also produces phase lag, both of them contribute to the instability of the control unit. In order to ensure the stability of the control system at higher frequencies, a phase lag compensator is required. In general, the compensator cannot perfectly make up the phase lag, as a consequence that the controller is similar to a low-pass filter in order to reduce the influence of signals at higher frequencies. In this work, an initial filter with phase restraint conditions is designed, and corresponding to this initial filter, Least Mean Square (LMS) method in the frequency domain has been used to design the first-order IIR filter, which can be solved by the *fdesign.arbmagnphase* function in Matlab. However, the amplitude of the initial filter is arbitrary, which may lead to the instability of the IIR filter. So *fmincon* function (Matlab), namely the active-set method, is used to optimize it. The frequency response of the final IIR filter is shown in Fig. 10. The compensator acts as a low-pass filter to reduce the non-collocated effect of the sensor and actuator pair at higher frequencies. Also, the phase–frequency response function of the controller increases up to -43° at 10k Hz, in order to make up the phase lag and enhance the stability of the control system.

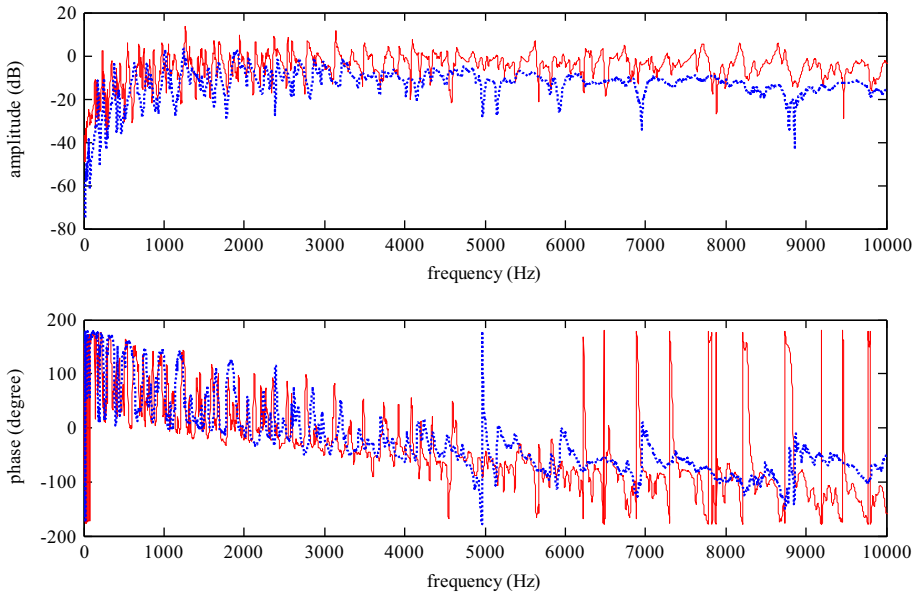

Fig. 9. Experimental open loop frequency response function of a sensor/actuator pair (1–10k Hz). Standard panel (dashed line) and thinner panel (solid line).

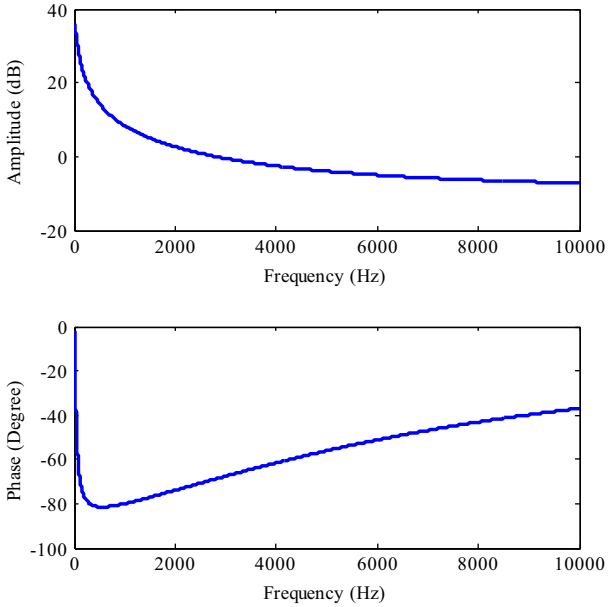

Fig. 10. The frequency response of filter.

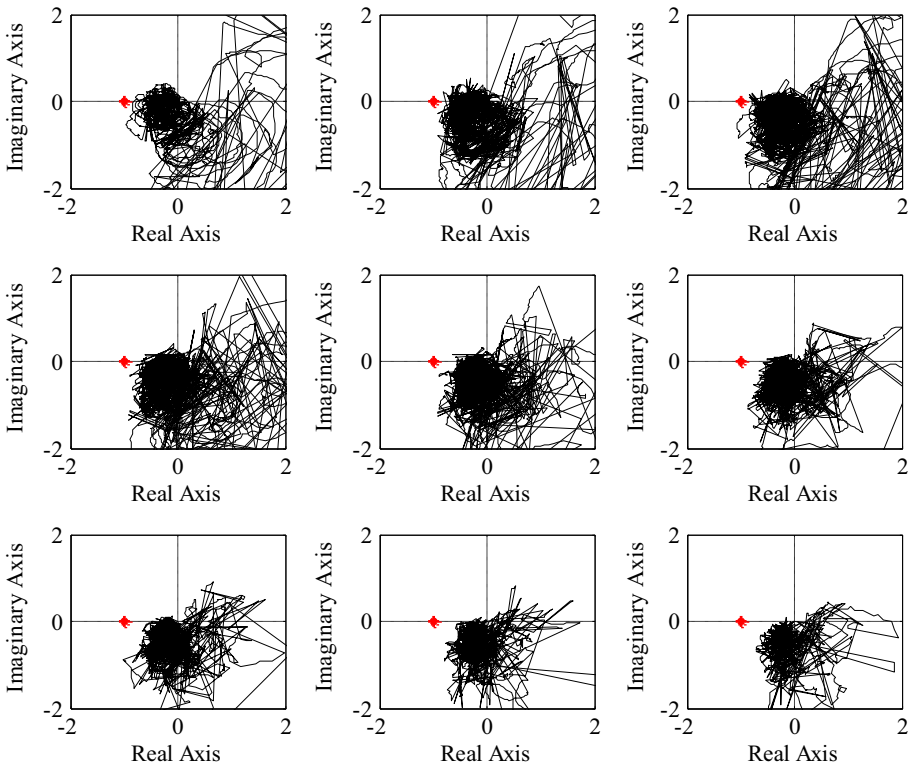

Fig. 11. The nine channels eigenvalues loci of matrix $\mathbf{G}(j\omega)\mathbf{H}(j\omega)$ (1–10k Hz).

4.4. Stability assessment

As shown in Fig. 5, the matrix $\mathbf{G}(j\omega)$ is the transfer function matrix between the sensors output and the actuators input. The control system is decentralized and the feedback control function $\mathbf{H}(j\omega)$ is diagonal. The stability of the multi-channel decentralized feedback control system has been assessed by the eigenvalues loci of the open loop frequency response matrix $\mathbf{G}(j\omega)\mathbf{H}(j\omega)$ in a frequency range of 1–10k Hz, and the nine channels eigenvalues loci are shown in Fig. 11. It can be noticed

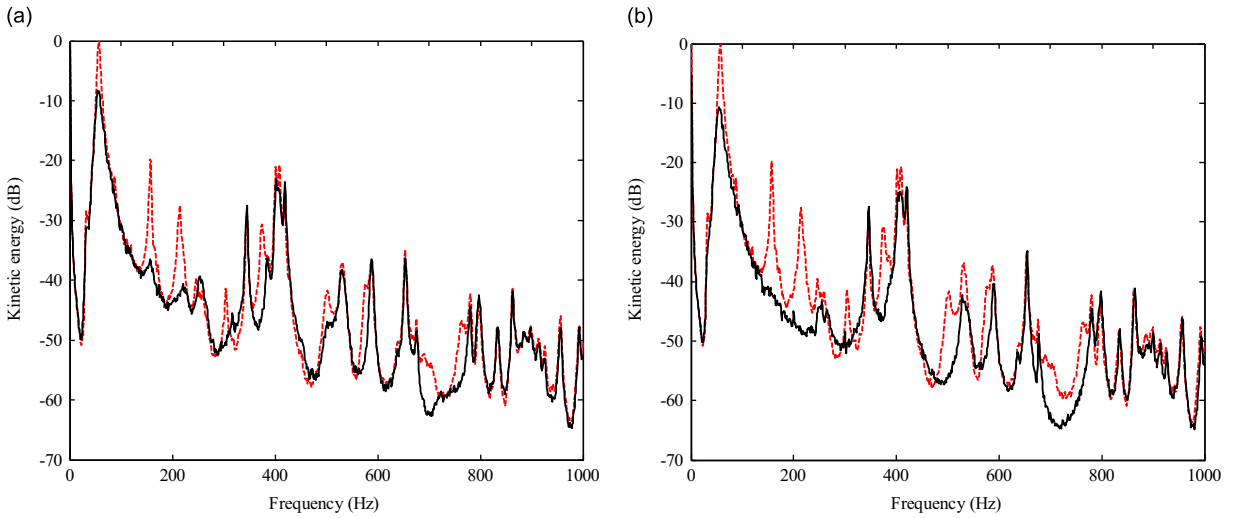

Fig. 12. The kinetic energy of the plate with the excitation of the loudspeaker in the cavity between 1 and 1k Hz without control (dashed line), and when the 2 control loops (a), 9 control loops (b) are implemented (solid line).

that all the loci do not enclose the Nyquist point $(-1, 0)$ at the frequency band of 1–10k Hz, which proves that the multi-channel feedback control system is stable with the given optimal feedback gain. The least gain margin is 1.8 dB, which is calculated by the first plot in Fig. 11. Actually, when the fourth and fifth channels are not added to the control system, the gain margin is about 5.3 dB. Thus, the gain margin is different for different channels.

5. Control results

In this section, the optimal feedback gain obtained by maximizing virtual absorbed energy and the designed digital phase lag compensator, as mentioned above, are applied in this multichannel feedback control system. The control results under different conditions are presented as follows. When the optimal control gains are implemented, the response at high frequency increases due to feedback spillover, but the control system can still be stable and the kinetic energy of the panel is reduced.

5.1. Control performance with different number of control loops

In this work, control performances with different number of control loops are investigated. The total kinetic energy of the plate has been measured between 1 and 1k Hz, where reductions of 5.5 dB, 5.8 dB, 6.5 dB, and 7.5 dB for 2 control loops (units 5 and 7), 4 control loops (units 2, 3, 5 and 7), 6 control loops (units 1, 2, 5, 7, 8 and 9), and 9 control loops are achieved respectively. In this system, the first mode of the panel with the coupling cavity holds the main vibration energy, and the other odd–odd modes of the panel also have many resonance peaks in the kinetic energy curves, thus the 5th control unit is the most important secondary source in this feedback control system. With the other channels added, the additional noise reduction is comparatively smaller. For brevity, only the results for two control loops and nine control loops are given in Fig. 12 which shows the kinetic energy of the plate measured by 12 error sensors. In Fig. 12(a), the optimal feedback gain is implemented, and the least gain margin of the two controllers is 4.4 dB. For Fig. 12(b), the least gain margin of the nine controllers is 1.8 dB.

In Fig. 12, the first three resonance peaks of dashed lines are associated with the modes of the panel (1,1), (3,1) and (1,3), which occur respectively at 57 Hz, 158 Hz, 215 Hz and are well coupled with the cavity low-frequency response. The three peaks are effectively controlled in these plots. In contrast, the resonances dominated by the cavity natural modes are not controlled [13]. For instance, the fourth resonance frequency, due to the natural mode of the cavity (1,0,0), which occurs at 345 Hz, cannot be controlled effectively by decentralized velocity feedback control. This could also explain the little reduction of the peak at about 429 Hz, which denotes the two natural modes of the cavity (0,1,0), and (0,0,1). At the frequencies of 532 Hz and 589 Hz, which represent the natural frequencies of two modes (3,3) and (5,1) respectively, more reduction can be achieved by 9 control loops. This is because the control units at the edges of the plate are added, especially units 2 and 8 which can effectively reduce the vibration of mode (5,1), compared to the control units located at the corner of the panel.

5.2. Control performance with different control locations

The first mode of plate has the most vibration energy, and acoustic radiation efficiency. Thus, the 5th control unit, which locates at the center of the panel, is considered to be the most important secondary source for vibration control of the first mode of the panel. Fig. 13 presents the control effects of the other two control loops which are units 2 and 7. It can be seen from Fig. 1 that the two control units are not located at the center of the panel. They have reduced the kinetic energy of the panel by 2.2 dB. It can be seen from Fig. 12(a) that units 5 and 7 have a reduction of 5.5 dB. The natural frequencies of the first several odd–odd modes of the panel can be found according to the resonance peaks in Figs. 12(a) and 13. Unit 5, which locates at the center of the mode shapes, can thus effectively control the odd–odd modes, and reduce the panel vibration energy, together with the radiated sound energy as well. The least gain margin of these two channels is 6.2 dB.

5.3. Control performance with different thickness plates

For a thin plate, as it is investigated in Section 4, the open loop frequency response function of the thinner plate produces more phase lag, which may contribute to the instability of the control system. To implement feedback control and guarantee the system stability, it generally requires reducing the feedback gain or the bandwidth of control loops, both of which may affect the control effectiveness. Fig. 14 presents two channels (channels 5 and 7) control results of a thinner plate with thickness of 1 mm. For the thinner plate, to ensure the stability of the control system, the optimal feedback gain cannot be achieved, thus the control system is performed with the feedback gain about 5 dB less than the optimal gain. The gain

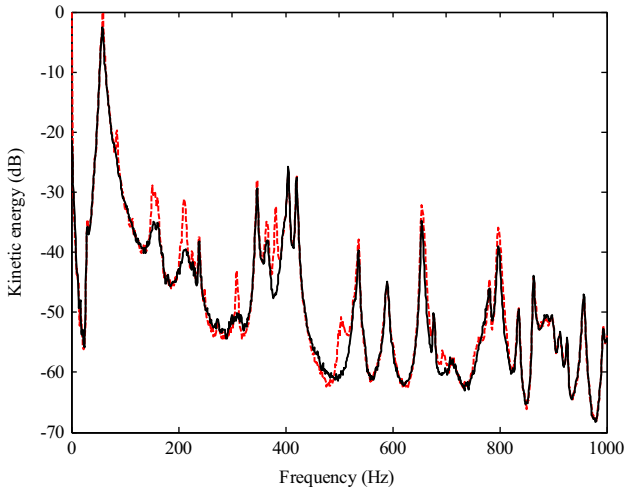

Fig. 13. The kinetic energy of the plate with two control units (units 2 and 7) (solid line), and without control (dashed line).

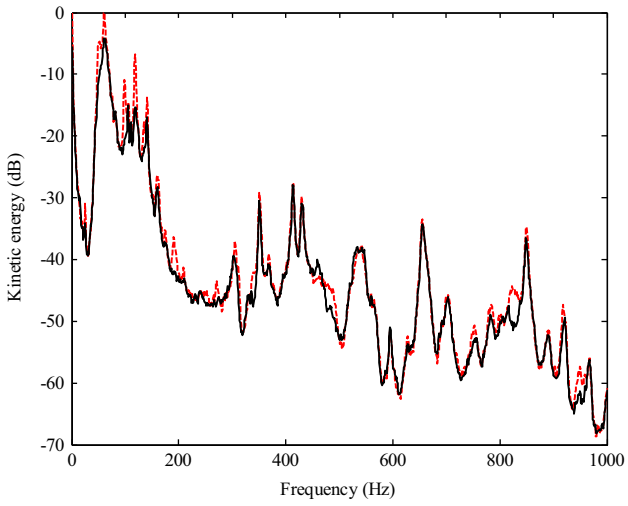

Fig. 14. The kinetic energy of a thinner plate (1 mm) with two control units (solid line), and without control (dashed line).

margin is less than 2 dB and the kinetic energy reduction is about 2.9 dB. In Fig. 14, the first several resonance peaks frequencies are close to each other. This is probably because the plate is not flat enough. Additionally, the coupling effect of the panel and cavity is stronger for the thinner panel, which may contribute to the larger shift of the natural frequencies. For the thicker plate, the optimal feedback gain can be achieved, and the kinetic energy reduction is about 5.5 dB which has been presented in Fig. 12(a) where the thickness of the plate is 1.8 mm. It can be found that a thicker plate can be controlled more effectively than a thinner one.

6. Conclusions

In this work, an experimental research on virtual absorbed energy for optimal feedback gain in decentralized velocity feedback control is implemented. It is proved that, compared with minimizing the kinetic energy, maximizing the virtual absorbed energy is able to obtain almost the same feedback gains in nine channels control system for broadband excitation, and is much more convenient to measure. Nine channels feedback loops with optimal feedback gains can reduce the total kinetic energy up to 7.5 dB for this experimental system. In addition, the experimental investigation on the open loop frequency response function shows that using smaller actuator and sensor, and relatively thicker panel can reduce the phase lag of the open loop frequency response function, and enhance the stability of the system. In a word, the virtual absorbed energy is a valid cost function for multichannel velocity feedback control for broadband excitation. However, when the bandwidth is reduced and the new first resonant peak is not included, the minimum of kinetic energy and the maximum of virtual absorbed energy do not match, which is the same as the theoretical results.

Acknowledgments

This work is supported by National Natural Science Foundation of China (Grant no. 11004216) and the Knowledge Innovation Program of Institute of Acoustics, Chinese Academy of Sciences.

References

[1] C.R. Fuller, S.J. Elliott, P.A. Nelson, *Active Control of Vibration*, Academic Press, London, 1996.
[2] P. Gardonio, S.J. Elliott, Smart panels for active structural acoustic control, *Smart Materials and Structures* 13 (2004) 1314–1336.
[3] C.R. Fuller, C.H. Hansen, S.D. Snyder, Active control of sound radiation from a vibrating rectangular panel by sound sources and vibration inputs: an experimental comparison, *Journal of Sound and Vibration* 145 (1991) 195–215.
[4] N. Hirami, Optimal energy absorption as an active noise and vibration control strategy, *Journal of Sound and Vibration* 200 (1997) 243–259.
[5] O. Bardou, P. Gardonio, S.J. Elliott, R.J. Pinnington, Active power minimization and power absorption in a plate with force and moment excitation, *Journal of Sound and Vibration* 208 (1997) 111–151.
[6] S.J. Sharp, P.A. Nelson, G.H. Koopmann, A theoretical investigation of optimal power absorption as a noise control technique, *Journal of Sound and Vibration* 251 (2002) 927–935.
[7] P.J. Remington, R.D. Curtis, R.B. Coleman, J.S. Knight, Reduction of turbulent boundary layer induced interior noise through active impedance control, *Journal of the Acoustical Society of America* 123 (2008) 1427–1438.
[8] M. Zilletti, S.J. Elliott, P. Gardonio, Self-tuning control systems of decentralized velocity feedback, *Journal of Sound and Vibration* 329 (2010) 2738–2750.
[9] M. Zilletti, S.J. Elliott, P. Gardonio, E. Rustighi, Experimental implementation of a self-tuning control system for decentralized velocity feedback, *Journal of Sound and Vibration* 331 (2012) 1–14.
[10] P. Gardonio, S. Miani, F. Blanchini, D. Casagrande, S.J. Elliott, Plate with decentralized velocity feedback loops: power absorption and kinetic energy considerations, *Journal of Sound and Vibration* 331 (2012) 1722–1741.
[11] M. Zilletti, P. Gardonio, S.J. Elliott, Optimisation of a velocity feedback controller to minimise kinetic energy and maximise power dissipation, *Journal of Sound and Vibration* 333 (2014) 4405–4414.
[12] Y. Cao, H.L. Sun, F.Y. An, X.D. Li, Virtual absorbed energy in decentralized velocity feedback control of a plate with piezoelectric patch actuators, *Applied Acoustics* 74 (2013) 909–919.
[13] P. Gardonio, E. Bianchi, S.J. Elliott, Smart panel with multiple decentralized units for the control of sound transmission. Part I: theoretical predictions, *Journal of Sound and Vibration* 274 (2004) 163–192.
[14] C. Hansen, S. Snyder, *Active Control of Noise and Vibration Volume II*, CRC Press, USA, 2013.
[15] S.S. Rao, *Vibration Measurement and Applications, Mechanical Vibration*, Addison-Wesley, USA, 1995.
[16] R.L. Clark, C.R. Fuller, A. Wicks, Characterization of multiple piezoelectric actuators for structural excitation, *Journal of the Acoustical Society of America* 90 (1991) 346–357.
[17] S.J. Kim, J.D. Jones, Optimal design of piezoactuators for active noise and vibration control, *AIAA Journal* 29 (1991) 247–263.
[18] S.E. Burke, J.E. Hubbard Jr., J.E. Meyer, Distributed transducers and collocation, *Mechanical Systems and Signal Processing* 7 (1993) 765–770.
[19] J.Q. Sun, Some observations on physical duality and collocation of structural control sensors and actuators, *Journal of Sound and Vibration* 194 (1996) 765–770.
[20] M.J. Balas, Direct velocity feedback of large space structures, *Journal of Guidance and Control* 2 (1979) 252–253.
[21] P. Gardonio, S.J. Elliott, Modal response of a beam with a sensor–actuator pair for the implementation of velocity feedback control, *Journal of Sound and Vibration* 284 (2005) 1–22.